HHS Public Access

Author manuscript

ACS Appl Nano Mater. Author manuscript; available in PMC 2020 August 28.

Published in final edited form as:

ACS Appl Nano Mater. 2018 ; 1(10): 5389–5395. doi:10.1021/acsanm.8b01380.

Free-Floating 2D Nanosheets with a Superlattice Assembled from Fe_3O_4 Nanoparticles for Peroxidase-Mimicking Activity

Ren Cai[†,‡], **Dan Yang**[§], **Liang Yan**[⊥], **Feng Tian**[‖], **Jichao Zhang**[‖], **Yifan Lyu**[‡,%], **Kangfu Chen**[▽], **Chengyi Hong**[†], **Xigao Chen**[†], **Yuliang Zhao**[⊥], **Zhuo Chen**[*,‡], **Weihong Tan**[*,†,‡]

[†]Center for Research at Bio/Nano Interface, Department of Chemistry and Department of Physiology and Functional Genomics, Health Cancer Center, UF Genetics Institute and McKnight Brain Institute, University of Florida, Gainesville, Florida 32611-7200, United States

[‡]Molecular Science and Biomedicine Laboratory, State Key Laboratory for Chemo/Bio Sensing and Chemometrics, College of Chemistry and Chemical Engineering, College of Life Sciences, and Aptamer Engineering Center of Hunan University, Hunan University, Changsha 410082, China

[‖]Shanghai Synchrotron Radiation Facility, Shanghai Institute of Applied Physics, Chinese Academy of Sciences, Shanghai 201204, China

[⊥]National Center for Nanoscience and Technology, Chinese Academy of Sciences, Beijing 100049, China

[§]School of Materials Science and Engineering, Nanyang Technological University, 50 Nanyang Avenue, Singapore 639798, Singapore

[▽]Department of Mechanical and Aerospace Engineering, University of Florida, Gainesville, Florida 32611-6250, United States

[%]Institute of Molecular Medicine, Renji Hospital, School of Medicine and College of Chemistry and Chemical Engineering, Shanghai 6 Jiao Tong University, Shanghai 200240, People's Republic of China

Abstract

The organization of nanoparticles (NPs) with controlled chemical composition and size distribution into well-defined sheets will find many practical applications, but the chemistry remains problematic. Therefore, we report a facile method to assemble NPs to free-floating two-dimensional (2D) nanosheets with a superlattice and thicknesses reaching 22.8 nm. The ligand oleic acid is critical in the formation of nanosheets. As assembled, these free-floating 2D nanosheets remain intact in both polar and nonpolar solvents, e.g., deionized water, ethanol, *N,N*-dimethylformamide, dimethyl sulfoxide, toluene, hexane, and chloroform, without any

[*]**Corresponding Authors:** tan@chem.ufl.edu., zhuochen@hnu.edu.cn.

Supporting Information

The Supporting Information is available free of charge on the ACS Publications website at DOI: https://doi.org/10.1021/acsanm.8b01380.

Characterization of Fe_3O_4 NPs and Fe_3O_4 NP–micelles, stability of 2D nanosheets, FTIR and ^1H NMR spectra, TEM image of hybrid 2D nanosheets, and comparisons of the kinetic parameters of Fe_3O_4 nanosheets and Fe_3O_4 NPs (PDF)

The authors declare no competing financial interest.

disassembly. Compared to Fe_3O_4 NP building blocks, these 2D nanosheets show more favorable catalytic properties and enhanced catalytic reactivity, which can be exploited to mimic natural enzymes. Our work is expected to open up a new avenue for synthesizing free-floating 2D supersheets by NP assembly, leading to a new generation of materials with enriched functions and broader applications.

Graphical Abstract

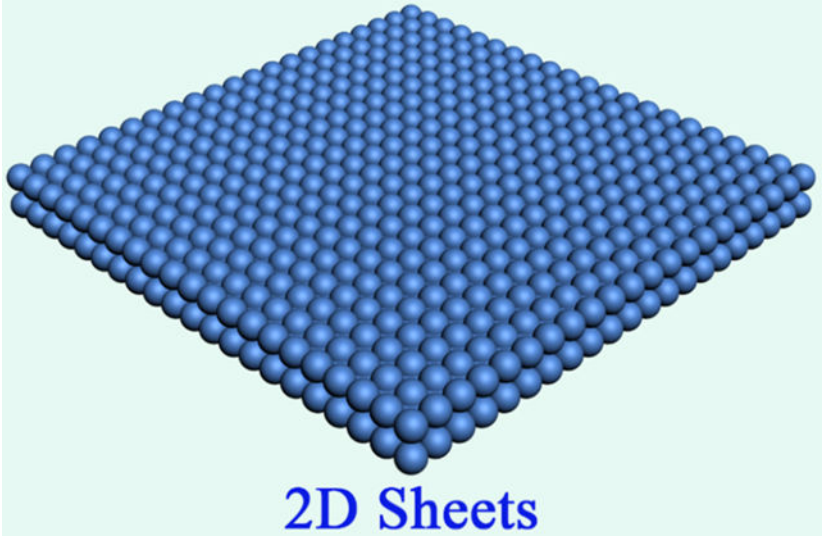

Keywords

superlattice; nanosheets; nanoparticles; self-assembly; catalysis

The assembly of nanoparticles (NPs) into higher-order architectures, e.g., one-, two-, or three-dimensional (1D, 2D, or 3D) superstructures, can result in materials with uniquely or synergistically enhanced properties,[1–4] and such materials have been used in many fields, including catalysis,[5] biomedical diagnosis,[6] sensors,[7] magnetic resonance imaging,[8] plasmonics,[9] and drug delivery.[10] Accordingly, various methods have been developed to fabricate assembled structures of different types and with different properties.[11,12] For example, binary superlattices prepared by the coassembly of PbTe and Ag_2Te NPs show higher electrical conductivity compared to those of each individual component (i.e., PbTe or Ag_2Te NPs).[13] An interfacial self-assembly approach was explored to prepare 2D metal chalcogenide semiconductors with a honeycomb superlattice through the oriented attachment of nanocrystals,[14] and a facile bottom-up process was employed to fabricate binary nanocrystal superlattices by the slow evaporation of colloidal dispersions on tilted substrates.[15] Through a reel-to-reel-compatible large-area-coating technique, diverse single-component and binary superlattices were formed by depositing colloidal nanocrystals onto various substrates.[16] Among these works, 2D structures by aligning NPs on specific substrates, or templates, have been reported,[17–19] but it remains a formidable challenge to achieve free-floating 2D sheets from NP assembly, e.g., stable 2D nanosheets with a superlattice, by a template/substrate-free assembly process.

Colloidal assembly is a well-known strategy to achieve hierarchical structure in two or three dimensions by manipulating NPs in solution.[20–22] On the basis of this strategy, we developed a facile route to fabricate free-floating 2D nanosheets with a superlattice and long-range ordering up to several micrometers (Scheme 1). The thicknesses of these nanosheets are around 22.8 nm when piled up by approximately three layers of NPs. Oleic acid (OA), one of the aliphatic ligands used to stabilize Fe_3O_4 NPs, is critical for the formation of well-defined nanosheets. It is noteworthy that these 2D nanosheets are stable and remain intact in both polar and nonpolar solvents. Compared to the original Fe_3O_4 NP building blocks, these 2D nanosheets show more favorable catalytic properties and enhanced catalytic reactivity, which could be quite promising for application in mimicking natural enzymes.

OA-stabilized Fe_3O_4 NPs (size ~7 nm; Figure S1) were prepared according to a previously reported method.[23] Then, an aqueous solution of cetyltrimethylammonium bromide (CTAB) was added to the above NP solution with vigorous stirring. A subsequent heating process evaporated the chloroform and transferred the NPs into the aqueous phase, forming an NP–micelle solution; then, the mixed solvent [diethylene glycol (DEG) and poly(vinylpyrrolidone) (PVP)] was injected into the as-prepared micelle solution. After the solution was held at 83 °C for 2 h, assembly of the NPs occurred. Finally, these products were isolated by centrifugation and redispersed in ethanol. Transmission electron microscopy (TEM) shows that as-prepared products are 2D nanosheets with lateral dimensions up to several micrometers (Figure 1a). These 2D nanosheets were washed, isolated by centrifugation, and redispersed in different solutions, which display the free-floating feature (Figure S2). The enlarged TEM image of one typical sheet in Figure 1b,c further reveals that it is composed of well-aligned NPs and shows a high degree of crystallinity (superlattice) with sharp electron diffraction spots (inset in Figure 1c). The thicknesses of 2D nanosheets were then measured by atomic force microscopy (AFM). The thickness of a typical sheet is 22.8 ± 0.5 nm, corresponding to approximately three layers of NPs (Figure 1d). The nanosheet exhibits on-axis superlattice–fringe patterns related to a face-centered-cubic (fcc) superlattice structure (Figure 1b,c), which was further investigated by an ensemble measurement of these nanosheets using small-angle X-ray scattering (SAXS). The SAXS data exhibit two distinguishable peaks that could be indexed as the (110) and (221) Bragg diffractions of an fcc structure with a lattice constant (a) of 8.7 ± 0.2 nm (Figure 1e), which is consistent with the value of 8.8 ± 0.2 nm obtained from the TEM images (Figure 1b,c). As confirmed by our experiments, these assembled nanosheets display excellent stability in different solvents, both polar and nonpolar, e.g. deionized water, ethanol, *N,N*-dimethylformamide, dimethyl sulfoxide, toluene, hexane, and chloroform (Figure S2).

For a better understanding of the growth mechanism of the nanosheets, reaction parameters were systematically tuned, and TEM was used to investigate the formation of these products. First, PVP and DEG work as a mixed solvent in this system. For instance, without PVP, no assembled product was collected. Second, CTAB works as a “wrapping” agent to form NP–micelles because the amphiphilic structure of CTAB mediated the interaction (dispersion) between NPs in the mixed solvent. Without CTAB, only irregular aggregates were formed (Figure S3). Third, OA is a very critical factor. Without OA as the ligand, Fe_3O_4 NPs easily

aggregated into bulk materials after injection into the mixed solvent (DEG and PVP; Figure 2b).[24] When the amount of OA was increased to 30 μL, monodispersed 3D particles composed of NPs were formed (Figure 2c). A further increase of OA to 35 μL resulted in the formation of semitransparent particles/vesicles (Figure 2d), which later merged together when 40 μL of OA was added (Figure S4b). With more OA added (50 μL), surface wrinkles, a characteristic feature of 2D sheets, could be clearly observed (Figure 2e). Finally, well-defined 2D sheets were achieved when 60 μL of OA was used (Figure 1). These results demonstrate that OA plays a critical role in avoiding the aggregation of large particles (Figure 2b), guiding the assembly of NPs to form monodispersed 3D particles (Figure 2c), and, finally, layering them into 2D sheets (Figure 2e,f).

On the basis of the above observations, we propose the following formation mechanism for free-floating 2D nanosheets with a superlattice (Figures 3 and 4). Prior to the assembly, Fe_3O_4 NP–micelles adopt an interdigitated bilayer structure with OA ligands as the inner layer and CTAB as the outer layer (Figure 3). This results from hydrophobic van der Waals interactions between the aliphatic chains of OA and CTAB.[25] These NP–micelles are uniformly dispersed in a mixed solvent (DEG and PVP), owing to the amphiphilic nature of CTAB (Figure 4a). During the heating process (83 °C and 2 h), with subsequent evaporation of chloroform, the CTAB layer (outer layer, Figure 3b) detaches from the surface of Fe_3O_4 NP–micelles because of its increased solubility in the mixed solvent upon heating, leaving OA-capped NPs “wrapping” inside the solvent (Figure 4b). ^{1}H NMR and FTIR spectra confirmed the self-dissociation of the CTAB layer and the presence of OA (Figures S5 and S6). When the OA volume is less than 30 μL (Figure 2f), a few OA molecules adsorb onto the surface of the Fe_3O_4 NPs (Figure 3a),[26] and these NPs tend to assemble into large particles (Figure 2b) because of the strong van der Waals attraction among NPs. The addition of more OA (35–40 μL) promotes the dispersion of NPs inside the mixed solvent, and the distance between NPs gradually increases, resulting in the swelling of 3D particles, as shown in Figure 4c, and, in turn, forming semitransparent vesicles, as shown in Figure 2d and S4b. A further increase of OA (50–60 μL) results in breakage of the particle vesicles, and free-floating nanosheets (Figures 2e and 1), namely, fragments of the broken vesicles, are formed. It is worth noting that the redundant OA adsorbed on the surface of the NPs (Figure 3a)[27] acts as a “lubricating agent” to alleviate strong inter-NP attractions during the rearrangement process (Figure 4c).[28,29]

As a demonstration of one potential application for 2D nanosheets, we tested the peroxidase-mimicking activities of Fe_3O_4 nanosheets, using 3,3′,5,5′-tetramethylbenzidine (TMB) and hydrogen peroxide (H_2O_2) as substrates. After the addition of Fe_3O_4 nanosheets to the TMB–H_2O_2 solution (pH 4.5), the solution changed from colorless to deep blue within 5 min at room temperature, as shown by the photograph and UV/vis absorption curves in Figure 5a,b. The optimum pH and temperature for catalysis of Fe_3O_4 nanosheets are approximately 4.5 and 25 °C, respectively, which are very close to the values of the natural enzyme horseradish peroxidase (HRP; Figure 5c,d).[30] The data in Figure 5e-h confirm that the catalytic activity of the Fe_3O_4 nanosheets is better than that of their Fe_3O_4 NP building blocks. As further revealed by the kinetic parameters presented in Table S1, K_m (Michaelis constant) is an indicator of the enzymatic affnity to the substrate, with a low K_m representing strong affnity and vice versa.[31] With H_2O_2 as the substrate, the apparent K_m value is about

20 times lower than that with HRP as the substrate,[30] and the initial velocity (V_{max}) is about 2 times greater, indicating a better affnity between H_2O_2 and Fe_3O_4 nanosheets compared to that of HRP. This can be ascribed to the collective property of the building blocks, leading to more active sites for H_2O_2 interaction (Table S1),[32] which, in turn, results in lower K_m and higher V_{max}. These results show that the 2D nanosheets could serve as a better artificial enzyme system than Fe_3O_4 NPs or the natural enzyme HRP.

In conclusion, we have developed a template-free assembly route to fabricate free-floating 2D nanosheets with a superlattice from NPs. By fine-tuning aliphatic ligands, NPs can be effectively assembled into 2D nanosheets with lateral dimensions of several micrometers and thicknesses reaching 22.8 nm, and they display distinct superlattice structures. As a proof of concept, an artificial enzyme system composed of 2D nanosheets exhibits higher catalytic peroxidase activity compared to that of their building blocks and demonstrates functional mimicry of a natural enzyme. As revealed by these results, the flexible fabrication of free-floating 2D nanosheets from simple building blocks can be achieved. The success of this work will open a new avenue toward the design of stable and free-floating nanosheets, which will broaden the application of a new generation of functional materials.

Supplementary Material

Refer to Web version on PubMed Central for supplementary material.

ACKNOWLEDGMENTS

The authors are grateful to Dr. Kathryn Williams and Dr. Tie Wang for their critical comments during the preparation of this manuscript. The authors appreciate support from the BL16B1 beamline of the Shanghai Synchrotron Radiation Facility. This work is supported by NIH GM R35 127130 and NSF 1645215, and by NSFC grants (NSFC 21521063).

REFERENCES

(1). Mehdizadeh Taheri S; Michaelis M; Friedrich T; Förster B; Drechsler M; Römer FM; Bösecke P; Narayanan T; Weber B; Rehberg I; Rosenfeldt S; Förster S Self-assembly of Smallest Magnetic Particles. Proc. Natl. Acad. Sci. U. S. A 2015, 112, 14484–14489. [PubMed: 26554000]

(2). Singh G; Chan H; Baskin A; Gelman E; Repnin N; Kral P; Klajn R Self-assembly of Magnetite Nanocubes into Helical Superstructures. Science 2014, 345, 1149–1153. [PubMed: 25061133]

(3). Wang T; Zhuang J; Lynch J; Chen O; Wang Z; Wang X; LaMontagne D; Wu H; Wang Z; Cao YC Self-Assembled Colloidal Superparticles from Nanorods. Science 2012, 338, 358–363. [PubMed: 23087242]

(4). Jones MR; Seeman NC; Mirkin CA Programmable Materials and the Nature of the DNA Bond. Science 2015, 347 (6224), 1260901. [PubMed: 25700524]

(5). Chen C; Nan C; Wang D; Su Q; Duan H; Liu X; Zhang L; Chu D; Song W; Peng Q; Li Y Mesoporous Multicomponent Nanocomposite Colloidal Spheres: Ideal High-Temperature Stable Model Catalysts. Angew. Chem., Int. Ed 2011, 50, 3725–3729.

(6). Zhu G; Hu R; Zhao Z; Chen Z; Zhang X; Tan W Noncanonical Self-Assembly of Multifunctional DNA Nanoflowers for Biomedical Applications. J. Am. Chem. Soc 2013, 135, 16438–16445. [PubMed: 24164620]

(7). Zheng Y; Thai T; Reineck P; Qiu L; Guo Y; Bach U DNA-Directed Self-Assembly of Core-Satellite Plasmonic Nanostructures: A Highly Sensitive and Reproducible Near-IR SERS Sensor. Adv. Funct. Mater 2013, 23, 1519–1526.

(8). Chen O; Riedemann L; Etoc F; Herrmann H; Coppey M; Barch M; Farrar CT; Zhao J; Bruns OT; Wei H; Guo P; Cui J; Jensen R; Chen Y; Harris DK; Cordero JM; Wang Z; Jasanoff A; Fukumura D; Reimer R; Dahan M; Jain RK; Bawendi MG Magneto-Fluorescent Core-shell Supernanoparticles. Nat. Commun 2014, 5, 5093. [PubMed: 25298155]

(9). Chen H; Shao L; Li Q; Wang J Gold Nanorods and Their Plasmonic Properties. Chem. Soc. Rev 2013, 42, 2679–2724. [PubMed: 23128995]

(10). Chou LYT; Zagorovsky K; Chan WC W. DNA Assembly of Nanoparticle SuPerstructures for Controlled Biological Delivery and Elimination. Nat. Nanotechnol 2014, 9, 148–155. [PubMed: 24463361]

(11). Shi Q; Dong D; Si KJ; Sikdar D; Yap LW; Premaratne M; Cheng W Shape Transformation of Constituent Building Blocks within Self-Assembled Nanosheets and Nano-origami. ACS Nano 2018, 12, 1014–1022. [PubMed: 29303252]

(12). Shi Q; Si KJ; Sikdar D; Yap LW; Premaratne M; Cheng W Two-Dimensional Bipyramid Plasmonic Nanoparticle Liquid Crystalline Superstructure with Four Distinct Orientational Packing Orders. ACS Nano 2016, 10, 967–976. [PubMed: 26731313]

(13). Urban JJ; Talapin DV; Shevchenko EV; Kagan CR; Murray CB Synergism in Binary Nanocrystal Superlattices Leads to Enhanced p-type Conductivity in Self-Assembled PbTe/Ag2Te Thin Films. Nat. Mater 2007, 6, 115–121. [PubMed: 17237786]

(14). Boneschanscher MP; Evers WH; Geuchies JJ; Altantzis T; Goris B; Rabouw FT; van Rossum SAP; van der Zant HSJ; Siebbeles LDA; Van Tendeloo G; Swart I; Hilhorst J; Petukhov AV; Bals S; Vanmaekelbergh D Long-range Orientation and Atomic Attachment of Nanocrystals in 2D Honeycomb Superlattices. Science 2014, 344, 1377–1380. [PubMed: 24948734]

(15). Smith DK; Goodfellow B; Smilgies D-M; Korgel BA Self-Assembled Simple Hexagonal AB_2 Binary Nanocrystal Super-lattices: SEM, GISAXS, and Defects. J. Am. Chem. Soc 2009, 131, 3281–3290. [PubMed: 19216526]

(16). Bodnarchuk MI; Kovalenko MV; Pichler S; Fritz-Popovski G; Hesser G; Heiss W Large-Area Ordered Superlattices from Magnetic Wustite/Cobalt Ferrite Core/Shell Nanocrystals by Doctor Blade Casting. ACS Nano 2010, 4, 423–431. [PubMed: 20028102]

(17). Miszta K; de Graaf J; Bertoni G; Dorfs D; Brescia R; Marras S; Ceseracciu L; Cingolani R; van Roij R; Dijkstra M; Manna L Hierarchical Self-assembly of Suspended Branched Colloidal Nanocrystals into Superlattice Structures. Nat. Mater 2011, 10, 872–876. [PubMed: 21946613]

(18). Lin Y; Thomas MR; Gelmi A; Leonardo V; Pashuck ET; Maynard SA; Wang Y; Stevens MM Self-Assembled 2DFree-Standing Janus Nanosheets with Single-Layer Thickness. J. Am. Chem. Soc 2017, 139, 13592–13595. [PubMed: 28902999]

(19). Albert SK; Sivakumar I; Golla M; Thelu HVP; Krishnan N; Libin KLJ; Ashish; Varghese, R. DNA-Decorated Two-Dimensional Crystalline Nanosheets. J. Am. Chem. Soc 2017, 139, 17799–17802. [PubMed: 29232955]

(20). Vogel N; Retsch M; Fustin CA; del Campo A; Jonas U Advances in Colloidal Assembly: The Design of Structure and Hierarchy in Two and Three Dimensions. Chem. Rev 2015, 115, 6265–6311. [PubMed: 26098223]

(21). Gong JX; Li GD; Tang ZY Self-assembly of Noble Metal Nanocrystals: Fabrication, Optical Property, and Application. Nano Today 2012, 7, 564–585.

(22). Qiu L; Chen T;Öçsoy I; Yasun E; Wu C; Zhu G; You M; Han D;Jiang J; Yu R; Tan W A Cell-Targeted, Size-photocontrollable, Nuclear-uptake Nanodrug Delivery System for Drug-resistant Cancer Therapy. Nano Lett 2015, 15, 457–463. [PubMed: 25479133]

(23). Li YZ; Ma FY; Su XT; Sun C; Liu JC; Sun ZQ; Hou YL Synthesis and Catalysis of Oleic Acid-coated Fe_3O_4Nanocrystals for Direct Coal Liquefaction. Catal. Commun 2012, 26, 231–234.

(24). Silvera Batista CA; Larson RG; Kotov NA Nonadditivity of Nanoparticle InterActions. Science 2015, 350, 1242477. [PubMed: 26450215]

(25). Fan H; Leve E; Gabaldon J; Wright A; Haddad RE; Brinker CJ Ordered Two- and Three-Dimensional Arrays Self-Assembled from Water-Soluble Nanocrystal-Micelles. Adv. Mater 2005, 17, 2587–2590.

(26). Yang K; Peng H; Wen Y; Li N Re-examination of Characteristic FTIR Spectrum of Secondary Layer in Bilayer Oleic Acid-coated Fe_3O_4 Nanoparticles. Appl. Surf. Sci 2010, 256, 3093–3097.

(27). Lan Q; Liu C; Yang F; Liu SY; Xu J; Sun DJ Synthesis of Bilayer Oleic Acid-coated Fe_3O_4 Nanoparticles and Their Application in pH-responsive Pickering Emulsions. J. Colloid Interface Sci 2007, 310, 260–269. [PubMed: 17382339]

(28). Min Y; Akbulut M; Kristiansen K; Golan Y; Israelachvili J The Role of Interparticle and External Forces in Nanoparticle Assembly. Nat. Mater 2008, 7, 527–538. [PubMed: 18574482]

(29). Ji T; Lirtsman VG; Avny Y; Davidov D Preparation, Characterization, and Application of Au-Shell/Polystyrene Beads and Au-Shell/Magnetic Beads. Adv. Mater 2001, 13, 1253–1256.

(30). Gao L; Zhuang J; Nie L; Zhang J; Zhang Y; Gu N; Wang T; Feng J; Yang D; Perrett S; Yan X Intrinsic Peroxidase-like Activity of Ferromagnetic Nanoparticles. Nat. Nanotechnol 2007, 2, 577–583. [PubMed: 18654371]

(31). Guo Y; Deng L; Li J; Guo S; Wang E; Dong S Hemin-Graphene Hybrid Nanosheets with Intrinsic Peroxidase-like Activity for Label-free Colorimetric Detection of Single-Nucleotide Polymorphism. ACS Nano 2011, 5, 1282–1290. [PubMed: 21218851]

(32). Cai R; Yang D; Peng S; Chen X; Huang Y; Liu Y; Hou W; Yang S; Liu Z; Tan W Single Nanoparticle to 3D Supercage: Framing for an Artificial Enzyme System. J. Am. Chem. Soc 2015, 137, 13957–13963. [PubMed: 26464081]

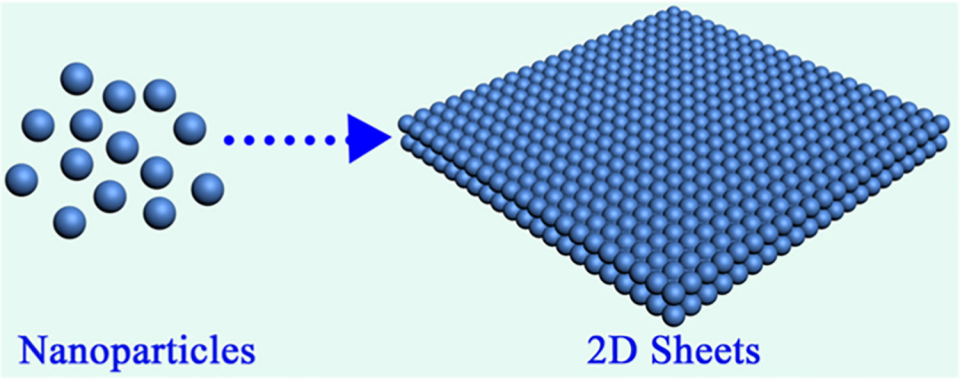

Scheme 1.
Formation of Free-Floating 2D Nanosheets through the Self-Assembly of NPs

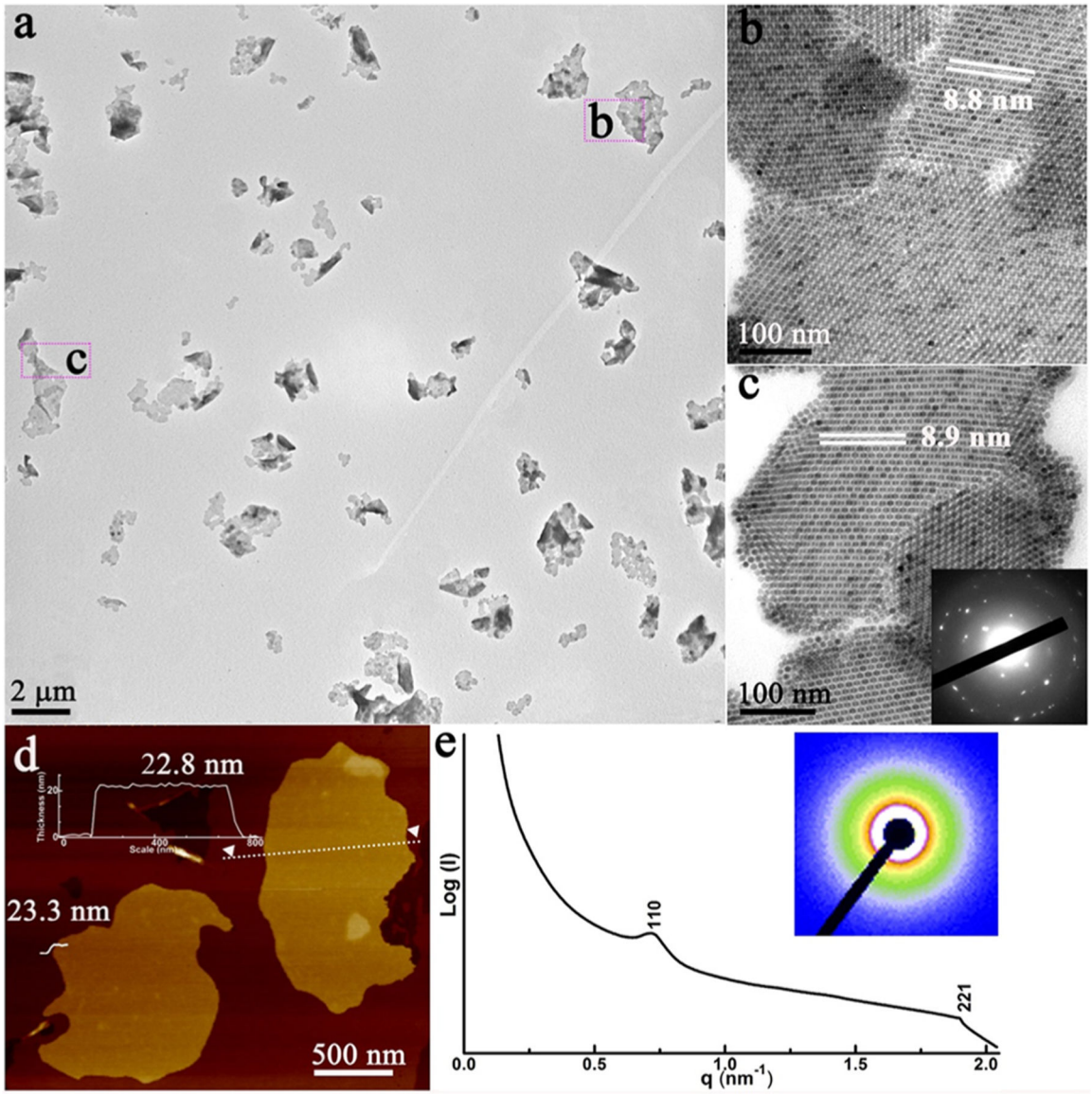

Figure 1.

Characterization of free-floating 2D nanosheets: (a) low- and (b and c) high-magnification TEM images and electron diffraction pattern (inset); (d) AFM image; (e) SAXS pattern (inset) of the 2D nanosheets, where the color scale indicates the intensity.

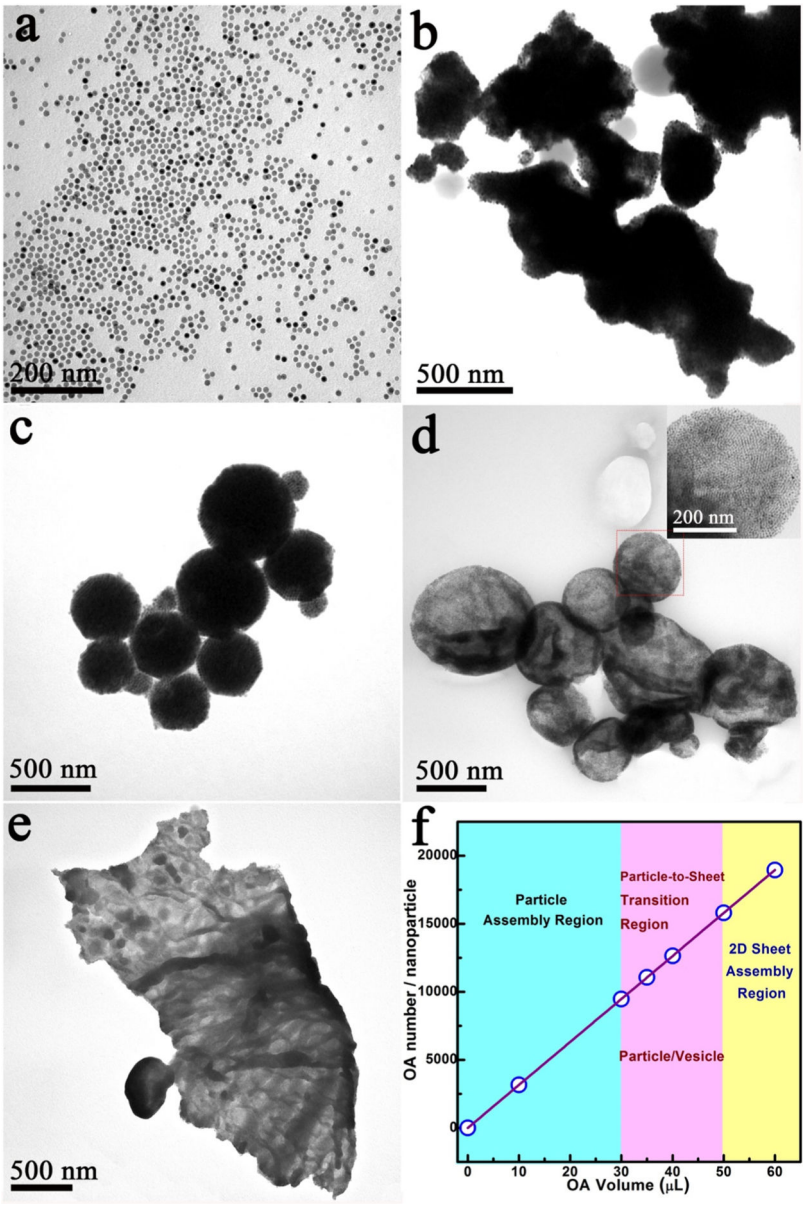

Figure 2.

TEM images of the assembly process for free-floating 2D nanosheet formation. Samples prepared from NPs assembled by adding different amounts of OA to guide the assembly process: (a) Fe_3O_4 NPs; (b) 0 μL; (c) 30 μL; (d) 35 μL; (e) 50 μL; (f) relationship between the OA amount and assembled structures.

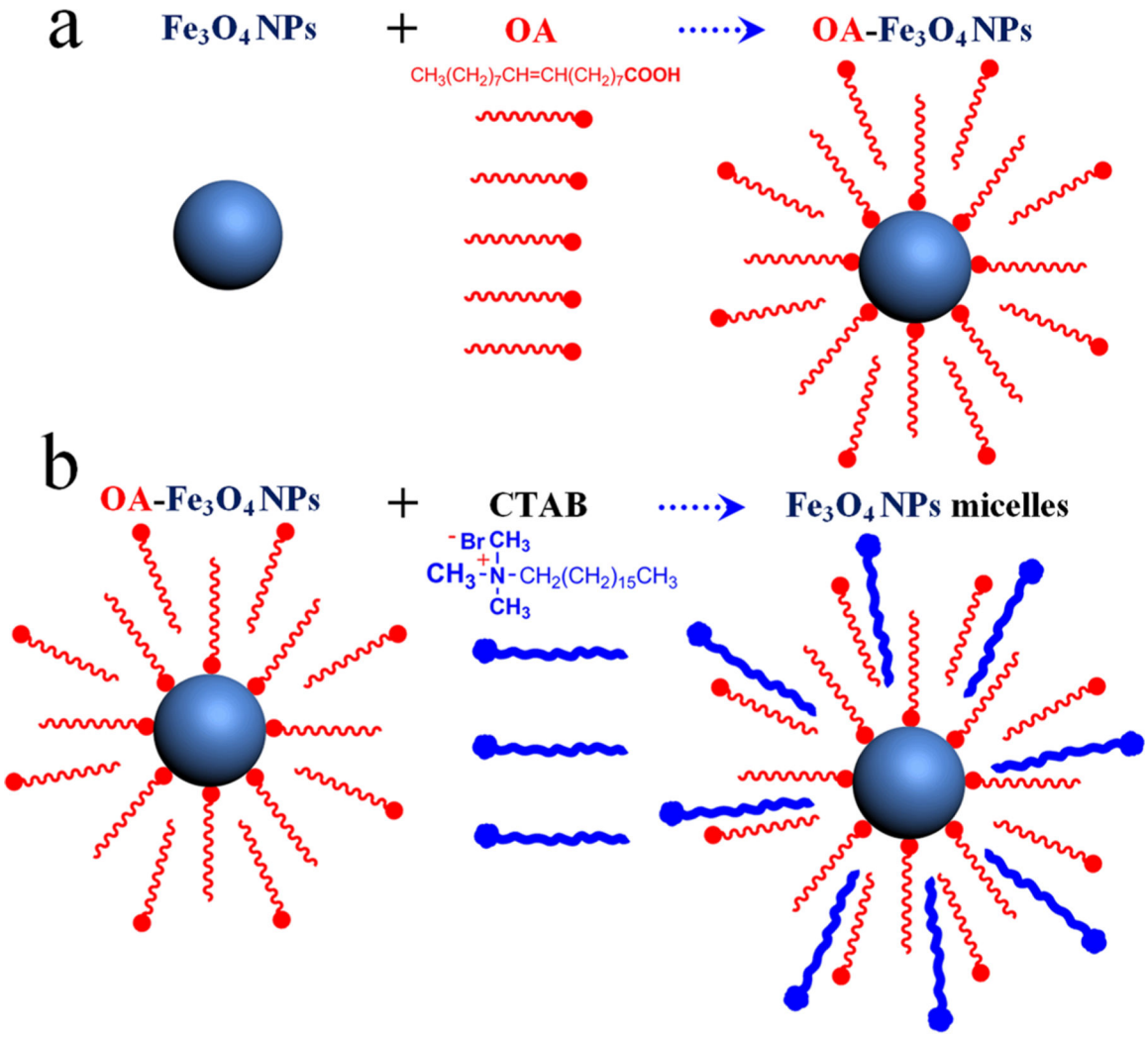

Figure 3.

Schematic illustration of Fe_3O_4 NP–micelles formation: (a) OA-stabilized Fe_3O_4 NPs; (b) Fe_3O_4 NP–micelles. These adopt an interdigitated bilayer structure with OA ligands as the inner layer and CTAB as the outer layer (when the OA volume is more than 30 μL, many more OA molecules adsorb onto the surface of the Fe_3O_4 NPs).

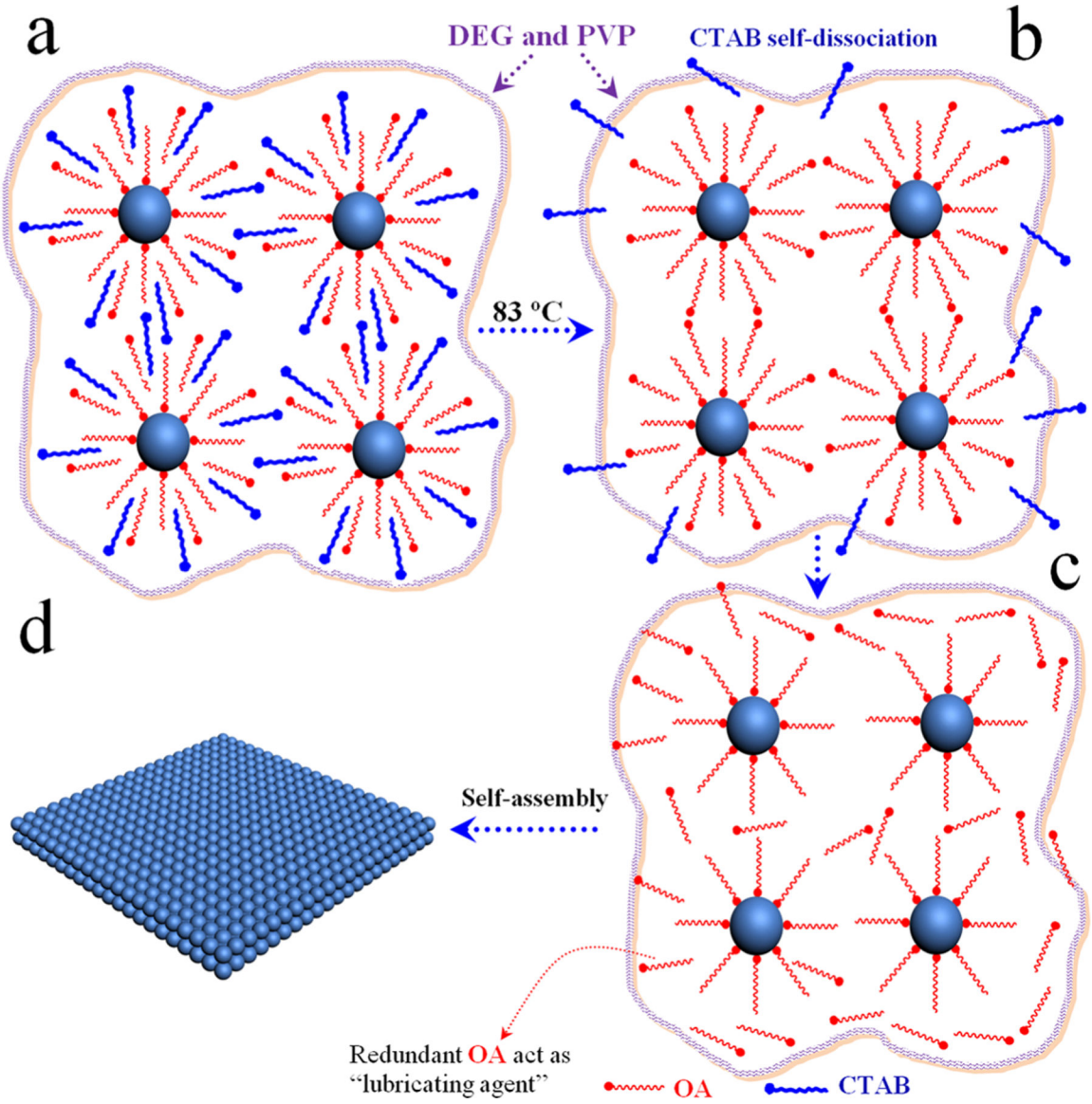

Figure 4.

Scheme of the free-floating 2D nanosheet assembly: (a) Fe_3O_4 NP–micelles in a mixed solvent; (b) self-dissociation of the CTAB layer;(c) OA acting as a "lubricating agent" to guide NP rearrangement; (d) formation of 2D nanosheets (the OA amount is 60 μL).

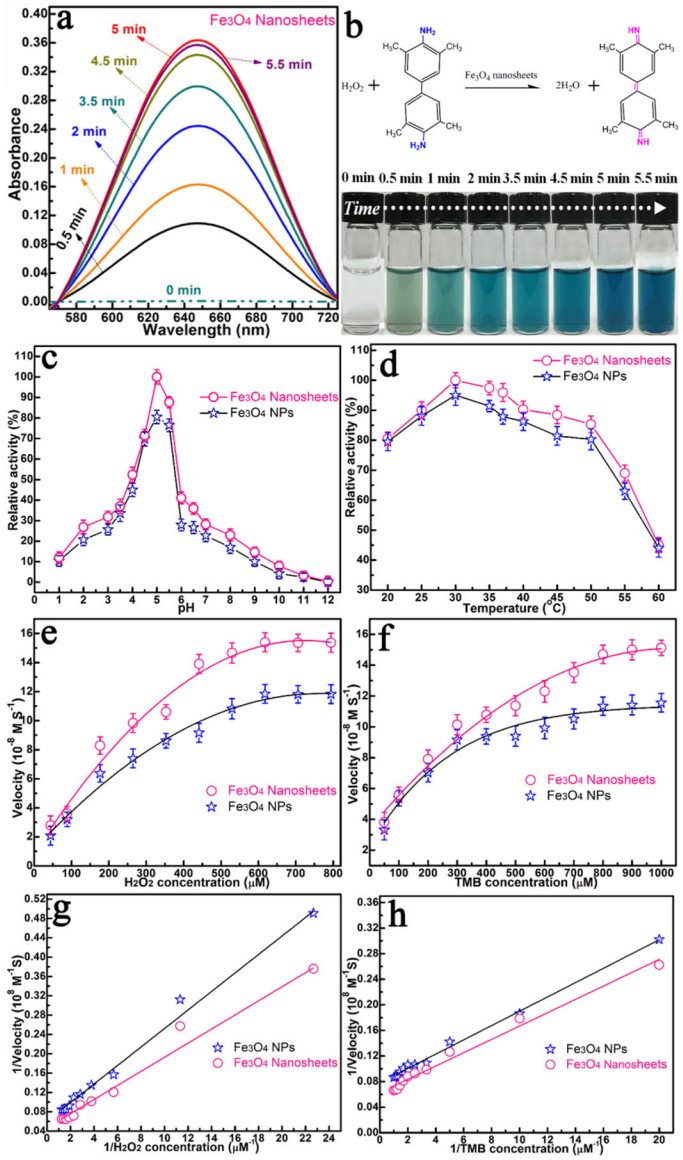

Figure 5.

(a) UV/vis spectra. (b) Photographs of Fe_3O_4 nanosheet catalysis using TMB as the substrate in the presence of H_2O_2 (pH 4.5 and 30 °C). (c) pH and (d) temperature dependences of the peroxidase-like activity of the Fe_3O_4 nanosheets and Fe_3O_4 NPs. The velocity of the reaction was measured using Fe_3O_4 NPs and Fe_3O_4 nanosheets. Fe_3O_4 nanosheets and Fe_3O_4 NPs show optimal pH and temperature of 4.5 and 30 °C, respectively. The maximum point in each curve was set as 100%. (e) Plot of the concentration of H_2O_2 at 530 μM and TMB concentration varied. (f) Plot of the concentration of TMB at 800 μM and H_2O_2 concentration varied. (g and h) Double-reciprocal plots with the concentration of one substrate (H_2O_2 or TMB) fixed and the other varied. Experimental conditions: 0.2 M sodium acetate (NaAc) buffer, pH 4.5, 30 °C.